Accepted version. The final version is available at: DOI 10.1109/TMTT.2017.2672547

Multi-State Multi-Resonator Spectral Signature Barcodes Implemented by Means of S-Shaped Split Ring Resonators (S-SRR)

Cristian Herrojo, *Student Member IEEE*, Ferran Paredes, *Member IEEE*, Javier Mata-Contreras, Simone Zuffanelli, *Member IEEE*, and Ferran Martín, *Fellow IEEE*

***Abstract*— Spectral signature barcodes functional at the S frequency band are presented in this paper. The barcodes are implemented by loading a coplanar waveguide (CPW) transmission line by means of multiple S-shaped split ring resonators (S-SRRs), each one tuned to a different frequency. The main particularity of this work is the fact that more than two logic states (i.e., three or four, depending on the implementation) are assigned to each resonant element. By this means, the total number of bits of the barcode (for a given number of resonators) is increased, as compared to previous approaches based on two logic states per resonator. This multi-state functionality is achieved by rotating the S-SRRs. Such rotation modulates the line-to-resonator coupling intensity, and consequently the notch depth at the S-SRR fundamental resonance. Therefore, by considering three or four fixed rotation angles (or orientations) between the line axis and the S-SRR (for the tri- and four-state multi-resonator barcodes, respectively), intermediate levels between the maximum and minimum attenuation, are achieved. This multi-state strategy only exploits a single frequency per resonant element (the fundamental one). Therefore, the data capacity per bandwidth is improved as compared to two-state based barcodes or to multi-state barcodes that use two frequencies per resonant element. As illustrative examples, two different four-state multi-resonator barcodes with eight S-SRRs (providing 4^8 = 65.536 different codes, or 16 bits) and with nine S-SRRs (equivalent to 18 bits), occupying a spectral bandwidth of 1 GHz and less than 6.75 cm^2 and 8.2 cm^2, respectively, are designed, fabricated and characterized.**

***Index Terms*– S-shaped split ring resonators (S-SRRs), coplanar waveguide (CPW) technology, spectral signature barcodes.**

I. Introduction

In radiofrequency identification (RFID) systems, objects or items are equipped with tags which communicate wirelessly with the interrogator or reader [1], [2]. RFID tags are typically composed of a compact antenna and an application specific integrated circuit (ASIC) that contains the ID code of the object or item. In UHF-RFID, read distances of various meters are usual, and line-of-sight for tag reading is not necessary. However, the presence of the microchip increases fabrication costs of the tag, and this limits the penetration of this technology in certain market segments [3].

This work was supported by MINECO-Spain (projects TEC2013-40600-R and RTC-2014-2550-7), *Generalitat de Catalunya* (project 2014SGR-157), *Institució Catalana de Recerca i Estudis Avançats* (who awarded F. Martín), and by FEDER funds. C. Herrojo acknowledges MINECO for supporting his research activity through the FPI grant BES-2014-068164.

The authors are with GEMMA/CIMITEC, Departament d'Enginyeria Electrònica, Universitat Autònoma de Barcelona, 08193 Bellaterra, Spain. E-mail: Ferran.Martin@uab.es.

To alleviate this problem, chipless tags have been proposed [3]-[5]. In chipless RFID, the tags are equipped with planar passive encoders, which can be implemented by means of low cost mass production fabrication techniques, including subtractive (etching) or printed (e.g., screen printing) techniques. However, such encoders represent a penalty in terms of tag size and data storage capacity. Although planar encoders cannot compete with microchips in these aspects (size and information capacity), their low cost fully justifies the research activity towards optimizing dimensions and number of bits.

This work is focused on multi-resonator transmission line based encoders, where a transmission line is loaded with multiple resonant elements (each tuned to a different frequency) [3], [6]-[8]. The tag code is inferred from the spectral signature of the loaded lines, given by a number of attenuation peaks (or notches) in the frequency response. The logic states '0' or '1' are determined by the absence or presence, respectively, of a notch at the resonance frequency of the resonators representing each bit of information. Such spectral signature barcodes, as they are usually designated, work in the frequency domain. Multi-resonator encoders based on the measurement of the radar cross section (RCS) have been also reported [9]-[14].

Other chipless tags use reflectors in a transmission line [15]-[19], and tag ID is obtained from the reflected pulses of a pulsed input signal. The spectral bandwidth is small, but the data storage capability is also small as compared to frequency domain based tags.

In order to decrease tag size and enhance the data storage capability (or number of bits) per frequency unit (a figure of merit) in multi-resonator spectral signature barcodes, a multi-state approach was proposed in [20]. Three logic states, rather than two, were assigned to each resonant element, an S-shaped split ring resonator (S-SRR) [21]-[23], thereby increasing the data capacity per resonant element. The use of S-SRRs is justified by their small electrical size, and by the fact that the logic states are simply achieved by properly orienting the resonator with regard to the line, as will be later discussed (S-SRR rotation was the principle for the implementation of angular displacement and velocity sensors, reported in [24]).

In this paper (an expanded version of [20]) we extend the number of states per resonator to four, by properly designing the S-SRRs and the host line, a coplanar waveguide (CPW). Moreover, we propose two different types of barcodes, one with the S-SRRs etched in the back

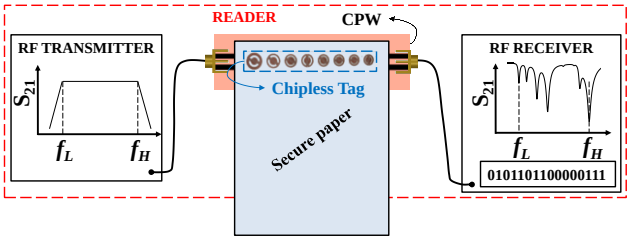

Fig. 1. Sketch of the chipless RFID system based on inductive coupling between the active part of the reader (CPW) and the tag (set of resonant elements). Note that the tag may be integrated within the tagged item (e.g., secure paper).

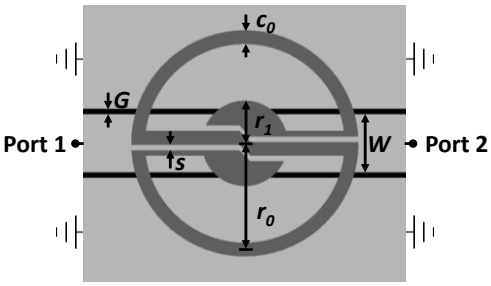

Fig. 2. Typical topology of an S-SRR-loaded CPW and relevant dimensions. The S-SRR is etched in the back substrate side.

substrate side of the CPW, and the other one with the S-SRRs etched in a different substrate. In the latter case, the one of interest in this work, the tag is simply the set of resonant elements etched, or printed, on the corresponding substrate. This substrate is different than the one where the transmission line is fabricated. The line can be considered to be part of the reader. Tag reading requires proximity and proper alignment between the line and resonant elements, and such reading is related to inductive coupling. In other words, we propose novel near-field chipless RFID tags that do not require antennas since the communication between the tag (set of resonators) and the reader (line) is by proximity. Such limitations (proximity and adequate orientation between tag and reader) are, however, compensated by two important aspects: (i) tag size (since antennas are not required), and (ii) data capacity per spectral bandwidth, due to the fact that up to four states per resonant element can be considered, as will be demonstrated in section III.C (note that losses in the wireless link prevent the application of these multi-state multi-resonator barcodes in far-field chipless RFID). In certain applications, such as security and authentication, tag size and number of bits are the main concerns. Optimization of these aspects at the expense of a reading system that ensures proximity and correct orientation between tag and reader (e.g., through a guiding system) can be accepted (see in Fig. 1 a scheme of the proposed system).

The paper is organized as follows. In section II, the working principle of these S-SRR-based multi-state multi-resonator barcodes is presented, and the design requirements for the resonant elements and the CPW host line are discussed by considering both the tri-state and four-state spectral signature barcodes. Section III is focused on the design examples. One example is an S-band encoder based on 10 tri-state resonators occupying an area of 860 mm^2 and 1 GHz spectral bandwidth, already presented in [20] but included here for completeness. Then, a pair of encoders implemented by means of eight and nine four-state S-SRRs, providing 16 and 18 bits, respectively, also occupying 1 GHz spectral bandwidth and an area of 675 mm^2 and 820 mm^2, are reported. In the encoder with 18 bits the S-SRRs and CPW are etched in the same substrate, and such encoder has been designed as a first step towards the 16-bit encoder with S-SRR etched on a separate substrate (the encoder of interest in this work for the reasons explained before). In section IV, the 16-bit encoder based on eight four-state S-SRRs is compared to other frequency domain encoders. Finally, the main conclusions are highlighted in Section V.

II. Working Principle, Design Requirements and Modeling

Coupling modulation between the host line and the resonant elements by rotation is the working principle of the proposed multi-state multi-resonator encoders [25], [26]. This principle was also applied to the design of angular displacement and velocity sensors [24], [27]-[30]. The key point is that for certain planar resonators, such as the S-SRR (see Fig. 2), their proximity to a host line, in our case a CPW transmission line, does not guarantee the appearance of line-to-resonator coupling. Fig. 3 depicts three different orientations of the S-SRR with regard to the CPW axis (the S-SRR is etched in the back substrate side). With the S-SRR orientation corresponding to Fig. 3(a), the magnetic field generated by the line is counter-directional in each S-SRR semi-loop, and the particle is excited. Consequently, a transmission zero at the fundamental S-SRR resonance is generated. The reason is that the currents at both halves (semi-loops) of the particle flow in opposite directions (clockwise and counterclockwise) at that frequency. Conversely, for an orientation angle of 90° [Fig. 3(b)], the net magnetic field in each resonator half (semi-loop) is negligible. Consequently, line-to-resonator coupling is very small, and signal attenuation at resonance is insignificant. By rotating the particle [Fig. 3(c)], the coupling level and hence the notch depth can be modulated. Consequently, three, or more, logic states per resonant element can be obtained by considering different angles between the S-SRR and the line.

It is worth to note that this functionality (coupling modulation) can be achieved with other resonant particles, in particular, with the electric LC (ELC) resonator [31]. Indeed, the ELC resonator is a bisymmetric particle, exhibiting a magnetic wall and an electric wall (both orthogonally oriented) at the fundamental resonance. When the magnetic wall of the ELC is aligned with the symmetry plane of the CPW transmission line, line-to-resonator coupling is maximized. However, by rotating the particle 90°, the electric wall of the ELC aligns with the symmetry plane of the line, and this prevents the appearance of coupling [28]. For different orientations, the coupling level and notch depth at resonance can be tailored to some extent, and the behavior is very similar to the one achievable with S-SRRs. However, the ELC is electrically much larger than the S-SRR, and for this main reason this particle (ELC) is discarded in this paper. The fact that the notch frequency does not experience a significant variation with the rotation angle is an important concern (if this is the case, overlapping with the resonance frequency of adjacent

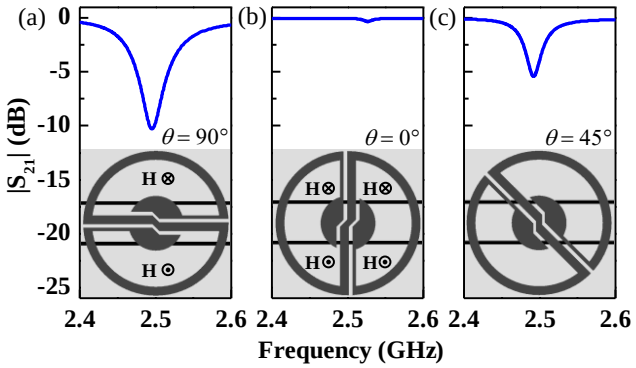

Fig. 3. Frequency responses for three different orientations between the S-SRR and the line to illustrate the working principle of the multi-resonator tags with more than two states per resonant element. (a) maximum coupling, (b) minimum coupling; (c) intermediate coupling.

resonators is avoided). In this regard, S-SRRs are useful particles since their resonance frequency is quite invariant with the rotation angle [24]. Therefore, S-SRRs are suitable particles for the implementation of multi-resonator barcodes.

Let us now discuss the specific topology of the S-SRR (Fig. 2). The circular shape is explained by the fact that this shape tends to linearize the response (notch depth in dB) with the rotation angle (we have thus considered in this application the notch depth in dB since roughly a linear dependence of the notch variation with the rotation angle is achieved). Note that the width of the loops is relatively wide, and the particle is terminated with semicircular patches (see central region). This topology results in relatively small S-SRR inductance and large S-SRR capacitance, and this is necessary to achieve significant notch depth for the maximum coupling state (90° rotation). Such notch depth should be large enough in order to be able to discriminate the intermediate states. Note however that by increasing the notch depth, the bandwidth per resonant element is also increased (because C_s/L_s increases). Therefore, a tradeoff is necessary. The S-SRR of Fig. 2 has been designed with an eye towards providing at least 10 dB attenuation (for the state corresponding to maximum coupling, i.e., with 90º orientation) and a maximum bandwidth (at half maximum) of 50 MHz. Such resonant particle has been designed to resonate at 2.5 GHz, and it is the reference S-SRR for the tri-state 10-resonator barcode first presented in [20], where resonance frequencies are separated by 100 MHz within the S frequency band (the spectral bandwidth covers the range 2 GHz - 3 GHz).

Fig. 4 shows the lossy simulation response of the structure of Fig. 2 for rotation angles of 45º and 90º, corresponding to the intermediate state and maximum coupling state, respectively (the substrate is *Rogers RO4003C* with thickness h = 0.81 mm, dielectric constant $\varepsilon_r = 3.55$ and $tan\delta = 0.0021$). These responses are appropriate to clearly discriminate the intermediate state, with a notch depth of roughly 5 dB, in contrast to the maximum attenuation of approximately 10 dB achieved by 90º S-SRR rotation. Note that the notch frequency for the 45º and 90º orientations scarcely varies.

The equivalent circuit model of the S-SRR-loaded CPW is depicted in Fig. 5(a) [24]. In this circuit, L and C are the inductance and capacitance, respectively, of the line, the S-

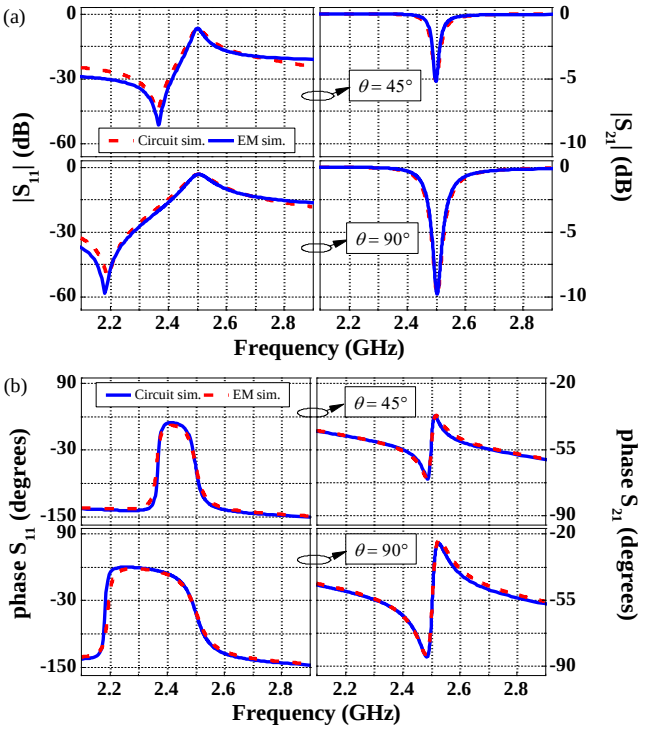

Fig. 4. Frequency response (including electromagnetic simulation and circuit simulation) of the CPW loaded with an S-SRR of Fig. 2 for different S-SRR angles. (a) Magnitude and (b) phase of the reflection (S_{11}) and transmission (S_{21}) coefficients. The electromagnetic simulations have been obtained with *Keysight Momentum*. S-SRR dimensions (in reference to Fig. 2) are: r_1 = 1.3 mm, r_0 = 3.4 mm, s = 0.2 mm, c_0 = 0.5 mm. Line dimensions are: W = 2.1 mm, G = 0.2 mm corresponding to a 50 Ω transmission line.

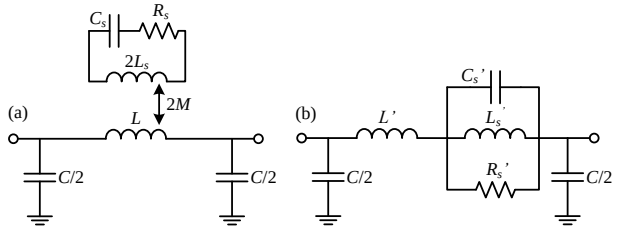

Fig. 5. Equivalent circuit model, including losses in the S-SRR, of the S-SRR-loaded CPW transmission line (a), and transformed model (b).

TABLE I
EXTRACTED ELEMENT VALUES OF THE CIRCUIT OF FIG. 5(b) FOR THE TRI-STATE S-SRR

θ (degrees)	L'_s (nH)	C'_s (pF)	R'_s (Ω)	L' (nH)	C (pF)
45	0.04	103	63.8	2.34	1.36
90	0.11	36.5	165	2.28	1.34

TABLE II
ELEMENT VALUES OF THE CIRCUIT OF FIG. 5(a) FOR THE TRI-STATE S-SRR

θ (degrees)	L_s (nH)	C_s (pF)	R_s (Ω)	L (nH)	M (nH)
45	10.0	0.20	3.05	2.38	0.44
90	10.0	0.20	3.31	2.39	0.74

SRR is accounted by the capacitance C_s and by the inductance of each loop, L_s, and the mutual inductance $2M$ describes the coupling between the line and the resonator. Contrary to previous works, we include in this model the losses of the S-SRR through the resistance R_s. The reason is that the notch depth (a relevant parameter) is related to losses. As discussed before, the mutual coupling depends on the relative orientation between the line and the resonator. Therefore, M is actually an angle dependent

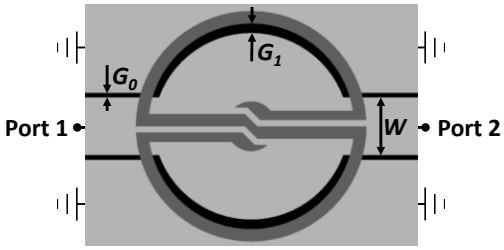

Fig. 6. Topology of a CPW transmission line section loaded with an S-SRR (etched in the back substrate side) corresponding to the reference resonant element of the four-state multi-resonator barcode, and relevant dimensions of the circularly shaped CPW: W = 1.85 mm, G_0 = 0.15 mm, G_1 = 0.31 mm corresponding to a 50 Ω transmission line.

parameter, or $M = M(\theta)$. The circuit of Fig. 5(a) can be transformed to the one indicated in Fig. 5(b), where the reactive elements of both models are related by [24]:

$$L_s^{'} = \frac{M^2}{2L_s} \tag{1}$$

$$C_s^{'} = \frac{4L_s^2 C_s}{M^2} \tag{2}$$

$$L^{'} = L - L_s^{'} \tag{3}$$

$$R_s^{'} = \frac{M^2}{2L_s C_s R_s} \tag{4}$$

We have extracted the parameters of the circuit of Fig. 5(b) from the electromagnetic responses corresponding to the 45º and 90º S-SRR orientations (see Table I). The method, reported in [32], is essentially based on the magnitude and phase response at certain frequencies, rather than on curve fitting. The circuit responses are also included in Fig. 4, and it can be appreciated that the agreement between electromagnetic and circuit simulation is good.

We have estimated the inductance of the S-SRR, L_s, by eliminating the central semicircular patches and by obtaining the reactance of the resulting structure, after connecting a differential port to the resulting terminals [28]. From the value of this inductance, i.e., L_s = 10 nH, we have then inferred the mutual inductance and the capacitance of the S-SRR. These S-SRR elements and the additional elements of the circuit of Fig. 5(a), inferred by inverting equations (1)-(4), are given in Table II. It can be seen that M is significantly larger for the 90º orientation, as expected. The other reactive parameters do not experience significant variations for both orientations, which is coherent with the proposed model, where the single angle dependent parameter is the mutual coupling. The un-loaded quality factor has been found to be 103 and 95 for the 45º and 90º orientations, respectively.

Let us now consider the requirements for the four-state multi-resonator barcodes. In this case, further notch depth (and hence coupling) for the maximum coupling state (90º) is necessary since two intermediate states are considered. To enhance the coupling, the transverse dimensions of the line in the region where the S-SRR are present, can be reshaped, resulting in a non-uniform transmission line. Specifically, the CPW transmission line is designed with circular and wider slots above the position of the S-SRRs (see the reference resonator/CPW in Fig. 6). By this means, the magnetic field lines generated by the CPW efficiently penetrate the area delimited by the semicircular halves of the S-SRR, enhancing the line-to-resonator coupling.

TABLE III
EXTRACTED ELEMENT VALUES OF THE CIRCUIT OF FIG. 5(b) FOR THE FOUR-STATE S-SRR

θ (degrees)	L'_s (nH)	C'_s (pF)	R'_s (Ω)	L' (nH)	C (pF)
25	0.03	135	60.9	2.46	1.59
50	0.08	47.3	175	2.45	1.57
90	0.18	22.3	356	2.35	1.51

TABLE IV
ELEMENT VALUES OF THE CIRCUIT OF FIG. 5(a) FOR THE FOUR-STATE S-SRR

θ (degrees)	L_s (nH)	C_s (pF)	R_s (Ω)	L (nH)	M (nH)
25	11.3	0.18	2.73	2.49	0.41
50	11.3	0.18	2.71	2.54	0.69
90	11.3	0.18	2.83	2.83	1.00

The S-SRR and the circularly shaped CPW of Fig. 6 have been designed so that for the state corresponding to maximum coupling, at least 15 dB of attenuation and less than 125 MHz bandwidth in the resulting notch are obtained. Such resonant particle has been designed to resonate at 2.5 GHz, and it is the reference S-SRR for the four-state nine-resonator (9 instead of 10 because the deeper the notch, the wider the bandwidth) barcode with S-SRRs and CPW etched in the same substrate. In these barcodes, to be presented later, resonance frequencies are separated by 125 MHz within the S frequency band (the spectral bandwidth covers the range 2 GHz - 3 GHz).

Fig. 7 shows the lossy simulated response of the structure of Fig. 6 for orientations of 25º, 50º and 90º, corresponding to the three considered states with significant coupling level (these values provide roughly equidistant notch depths). The substrate is *Rogers RO4003C* with thickness h = 508 μm, dielectric constant $\varepsilon_r = 3.55$ and $tan\delta = 0.0021$ (narrower than the one considered in the tri-state multi-resonator barcode, in order to enhance the line-to-resonator coupling). These responses are appropriate to discriminate the two intermediate states, corresponding to angles of 25º and 50º (note that the notch frequency is roughly the same in all the cases). We have extracted the parameters of the circuit of Fig. 5(b) from the electromagnetic responses corresponding to the 25º, 50º and 90º S-SRR orientations (see Table III). The circuit responses, also included in Fig. 7, are in good agreement with the electromagnetic simulations. Except M, the circuit elements of the circuit of Fig. 5(a), given in Table IV, are roughly invariant under rotation. By contrast, M exhibits roughly a linear dependence with θ, which is reasonable on account of the shape of the resonator and the line [28] (the variation is roughly linear if the resonator is circular, and this linearity is enforced if the CPW is circularly shaped as well).

Let us now focus on the relation between the geometry of the S-SRRs and the circuit model parameters. Obtaining analytical expressions is cumbersome on account of the complex geometry of the resonant particles and the presence of the CPW. Therefore, a parametric analysis has been carried out. It has been done by considering the structure of Fig. 2, with dimensions indicated in the caption of Fig. 4, and by varying either c_0 or r_1 with regard to the

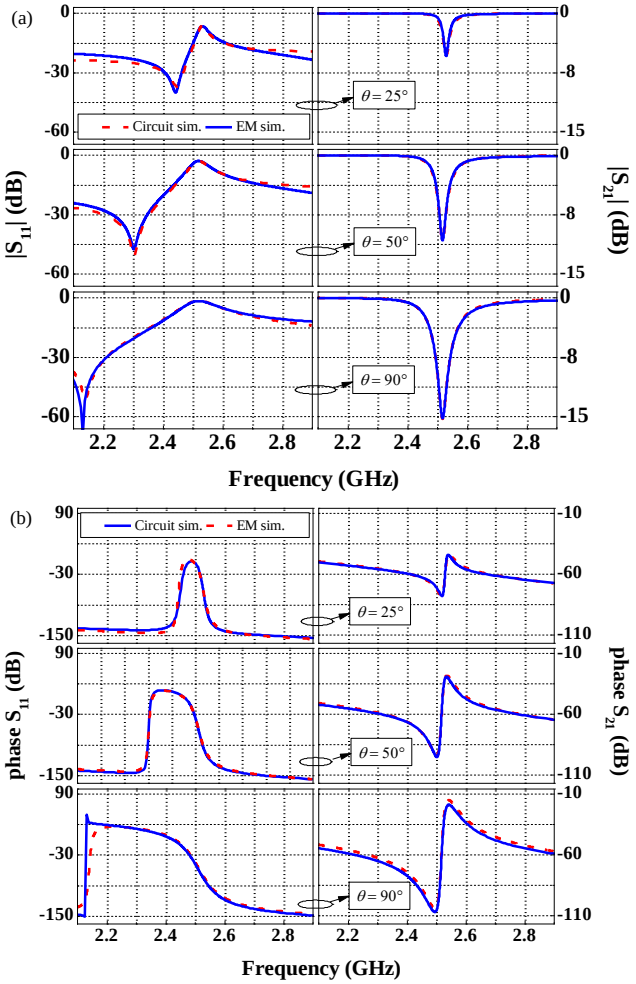

Fig. 7. Frequency response (including electromagnetic simulation and circuit simulation) of the S-SRR-loaded CPW of Fig. 6 for different angular orientations. (a) Magnitude and (b) phase of the reflection (S_{11}) and transmission (S_{21}) coefficients. The electromagnetic simulations have been carried out with *Keysight Momentum*. S-SRR dimensions (in reference to Fig. 6) are: r_1 = 0.8 mm, r_0 = 3.5 mm, s = 0.2 mm, c_0 = 0.4 mm. Line dimensions are: W = 1.85 mm, G_0 = 0.15 mm, G_1 = 0.31 mm corresponding to a 50 Ω transmission line.

values of Fig. 4. The orientation providing maximum attenuation (i.e., 90º) has been considered. The parameters of both circuit models [Figs. 5(a) and (b)] for different values of c_0 are given in Tables V and VI, whereas the effects of varying r_1 are summarized in Tables VII and VIII.

Essentially, the width of the loop, c_0, affects the inductance, L_s, and resistance, R_s, of the particle, whereas the radius of the central patches, r_1, has influence on the value of the capacitance, C_s, and resistance, R_s, as well. It is interesting to note that the notch depth (also included in the tables) is scarcely dependent on r_1, but it varies significantly with c_0. Therefore, according to this study, it follows that the width of the loops is a fundamental design parameter. For design purposes a tradeoff is necessary since, due to the limited Q-factor of the S-SRRs, it is not possible to achieve narrow band responses with deep notches. Necessarily, enhancing the notch depth means to widen the bandwidth. So the design process consists of varying c_0 until a reasonable notch depth and bandwidth is achieved. Then the S-SRR resonance frequency can be adjusted by the patch capacitance (through r_1) and also by the length of the loops. The length of the loops has mainly influence on L_s and R_s. In general, small loops are convenient to reduce R_s and to achieve small particle size, but the limit is dictated by the required value of L_s (or frequency).

TABLE V
EXTRACTED ELEMENT VALUES OF THE CIRCUIT OF FIG. 5(b) FOR DIFFERENT VALUES OF c_0

c_0	L'_s (pH)	C'_s (pF)	R'_s (Ω)	L' (nH)	C (pF)	S_{21} (dB)
0.2	91.0	50.9	135	2.34	1.26	-8.01
0.3	101	43.3	150	2.31	1.28	-8.73
0.4	105	39.8	161	2.33	1.32	-9.25
0.5	110	36.5	165	2.28	1.34	-9.49
0.6	114	34.1	167	2.29	1.36	-9.64
0.7	118	32.2	174	2.29	1.37	-9.98
0.8	119	31.4	176	2.28	1.39	-10.01

TABLE VI
ELEMENT VALUES OF THE CIRCUIT OF FIG. 5(a) FOR DIFFERENT VALUES OF c_0

c_0	L_s (nH)	C_s (pF)	R_s (Ω)	L (nH)	M (nH)
0.2	12.4	0.19	3.67	2.43	0.75
0.3	11.4	0.19	3.54	2.41	0.76
0.4	10.6	0.20	3.33	2.43	0.75
0.5	10.0	0.20	3.31	2.39	0.74
0.6	9.32	0.20	3.26	2.40	0.74
0.7	9.06	0.21	3.18	2.41	0.73
0.8	8.62	0.22	3.1	2.40	0.72

TABLE VII
EXTRACTED ELEMENT VALUES OF THE CIRCUIT OF FIG. 5(b) FOR DIFFERENT VALUES OF r_1

r_1	L'_s (pH)	C'_s (pF)	R'_s (Ω)	L' (nH)	C (pF)	S_{21} (dB)
0.7	104	31.3	166	2.28	1.35	-9.82
0.8	105	32.2	167	2.29	1.36	-9.85
0.9	107	32.7	168	2.29	1.35	-9.85
1.0	106	34.2	169	2.30	1.35	-9.82
1.1	111	33.9	170	2.29	1.34	-9.75
1.2	109	35.5	168	2.30	1.34	-9.65
1.3	110	36.5	165	2.28	1.34	-9.49

TABLE VIII
ELEMENT VALUES OF THE CIRCUIT OF FIG. 5(a) FOR DIFFERENT VALUES OF r_1

r_1	L_s (nH)	C_s (pF)	R_s (Ω)	L (nH)	M (nH)
0.7	10.0	0.16	3.91	2.38	0.72
0.8	10.0	0.17	3.74	2.39	0.72
0.9	10.0	0.17	3.64	2.40	0.73
1.0	10.0	0.18	3.46	2.41	0.73
1.1	10.0	0.19	3.52	2.40	0.74
1.2	10.0	0.19	3.36	2.41	0.74
1.3	10.0	0.20	3.31	2.39	0.74

III. DESIGN EXAMPLES AND POTENTIAL APPLICATIONS

Both tri- and four-state multi-resonator encoders are presented in this section on the basis of the reference S-SRRs and lines introduced in the previous section, where the S-SRRs are etched in the back substrate side of the CPW transmission line. Additionally, we present the design of a four-state S-SRR-based encoder implemented by etching the S-SRRs and the CPW transmission line in different substrates. Such encoders are of particular interest

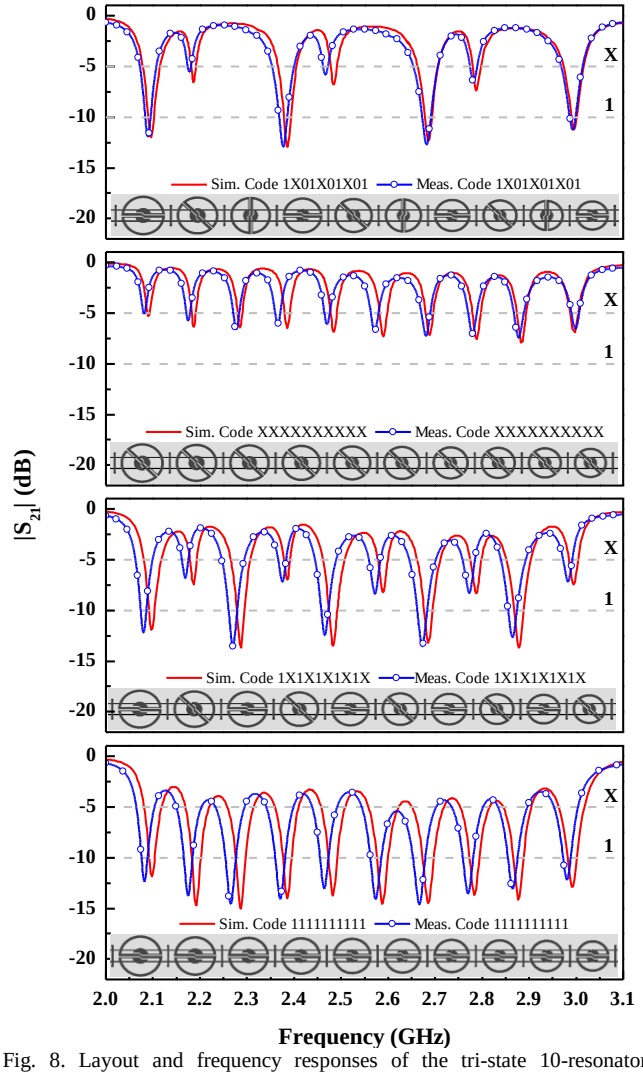

Fig. 8. Layout and frequency responses of the tri-state 10-resonator spectral signature barcodes with the indicated codes. The dots in the measured responses do not correspond to data points (1.600), but are used to better discern them from the simulated responses.

for certain applications where tag size and number of bits can be optimized (thanks to the use of multi-state resonators) at the expense of sacrificing long range reading (e.g., security, authentication, etc). Such encoders are those of interest in this paper, since it is in these encoders where the use of multi-state resonators is fully justified. In far-field chipless RFID, it is not realistic to distinguish between the different states mainly due to losses in the wireless link between the reader and the tags. By contrast, in this near-field based chipless RFID system, the CPW (which is part of the reader) must be in contact and conveniently aligned with the S-SRRs (the tag) and antennas are avoided in both the reader and the tag. This allows us to clearly discern between the four states, as will be later shown. Obviously, the alignment and proximity (contact) between the tag and the CPW transmission line for reading requires a guiding system, but this is not necessarily an issue in certain applications such as those indicated above.

A. Tri-state 10-resonator encoder

The implementation of the tri-state 10-resonator barcode has been done by scaling up or down the circumference perimeter of the S-SRR of Fig. 2, keeping unaltered the other dimensions. Such lengths have been calculated with the objective of achieving equidistant resonance frequencies (separated 100 MHz) between 2.1 GHz and 3.0 GHz. The layouts and simulated frequency responses (S_{21}) of four encoders with the indicated (arbitrary) codes are depicted in Fig. 8. We have used 'X' to designate the intermediate state (45°). As can be seen, the difference in attenuation level for states 'X' and '1' is significant, independently of the state of the neighbor S-SRRs.

The encoders of Fig. 8 have been fabricated through photo-mask etching. The measured responses are also depicted in Fig. 8. Note that by situating the thresholds at –5 dB and –10 dB, the three different states can be perfectly discerned (between 0 dB and the threshold level named X, the data reads as 0, between the level corresponding to the label X and 1, the data reads as X, and for notches deeper than the level of 1, the data reads as 1). Nevertheless, the notch level is unavoidably somehow influenced by the effects of the neighbor S-SRRs. For that main reason the notch depth is not identical for a given state, but the achieved results allow us to discern between the different states. With these encoders 3^{10} = 59.049 different codes can be generated (i.e., corresponding to more than 15 bits, or 2^{15} = 32.768 states). Area is small (i.e., 95 mm × 9 mm), and the information density per frequency (DPF), given by the number of bits per unit frequency is above 15 bits/GHz.

B. Four-state nine-resonator encoder

For the implementation of the four-state nine-resonator encoder from the reference structure of Fig. 6 (with S-SRR and CPW etched in the same substrate), we have increased or decreased the capacitance of the reference S-SRR in a tuning process focused on obtaining equidistant frequencies in the interval 2 GHz – 3GHz. The layouts and frequency responses of four encoders are depicted in Fig. 9 (the corresponding codes are indicated in the figure). The intermediate states are designated in this case by '01' and '10' for the 25º and 50º orientations, respectively, whereas the states '00' and '11' correspond to un-rotated and maximally rotated (90º) S-SRRs, respectively. The fabricated encoders exhibit the responses also depicted in Fig. 9. With these encoders, $4^9 = 2^{18}$ = 262.144 different combinations can be generated, corresponding to 18 bits. This number of combinations is substantially superior than the one of the previous tri-state based encoders, and size is smaller i.e., (91 mm × 9 mm) since 9 resonant elements, rather than 10, have been used.

The previous four-state (and tri-state) S-SRR-based encoders, with the resonant elements etched in the back substrate side of the CPW transmission line can be considered as preliminary prototypes of the S-SRR based encoder of interest in this work, to be discussed next.

C. Four-state eight-resonator encoder with S-SRRs and CPW etched in different substrate

Typically, multi-resonator barcodes (with two states per resonant element) have been equipped with cross polarized transmitter (TX) and receiver (RX) antennas (usually monopole antennas), in order to wirelessly communicate with the reader [6]-[8]. These chipless tags are thus composed by the S-SRRs and the CPW transmission line

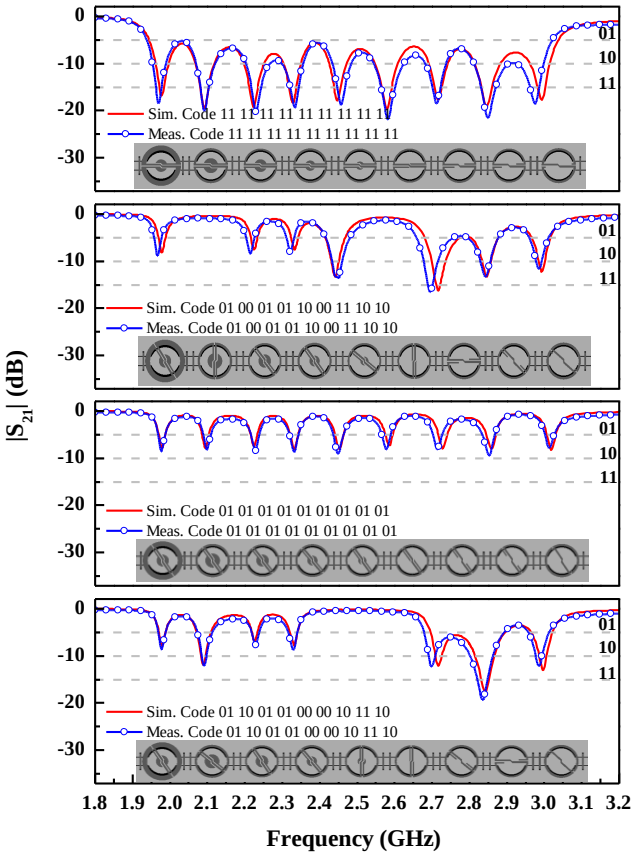

Fig. 9. Layout and frequency responses of the four-state nine-resonator spectral signature barcodes with the indicated codes. Between 0 dB and the threshold level named 01, the data reads as 00, between the level corresponding to the label 01 and 10, the data reads as 01, between 10 and 11, it reads as 10, and for notches deeper than the level of 11, the data reads as 11.

(the encoder), plus the TX and RX antennas, and the communication with the reader is via far-field.

A different configuration for multi-state multi-resonator encoders consists of implementing the CPW transmission line and the S-SRRs in a different substrate, as anticipated before. This makes sense if the CPW transmission line is considered to be part of the reader, while the spectral signature barcode is composed only by the set of S-SRRs, etched, or printed, on a different substrate (Fig. 1). The communication between the tag (set of S-SRRs) and the reader (CPW and the necessary electronics) is near-field in this case, and it is based on the inductive coupling between the CPW transmission line and the S-SRRs. Rather than contactless, the reader (CPW) and the tag (S-SRRs) must be in contact and aligned within this approach, but this is not an issue in certain applications, such as security, authentication, etc. Particularly, an application that can be envisaged is secure paper. The idea behind such application is that the paper is encoded with an S-SRR-based spectral signature (rather than with optical barcodes, easy to copy), buried on it. The code, i.e., the set of S-SRRs, can be printed on a flexible substrate or, even, directly on the final (paper) product. In order to perform identification, a robust guiding channel for the paper is necessary to guarantee the contact and alignment between the tag (S-SRRs) and the active part of the reader (CPW). Lateral misalignment between tag and CPW should be less than 0.3 mm, as demonstrated later. Note that in this application, a wireless link between the tag and the reader does not represent an

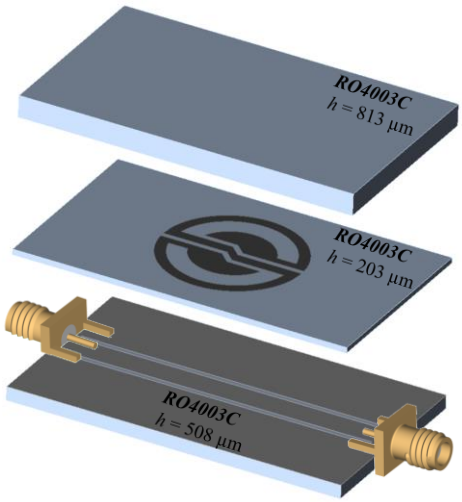

Fig. 10. Topology of the reference S-SRR of the 4-state multi-resonator barcode separated from the CPW transmission line, and relevant dimensions (values before scaling): r_1 = 1.5 mm, r_0 = 2.4 mm, s = 0.2 mm, c_0 = 0.4 mm. Line dimensions are: W = 1 mm, G = 0.2 mm corresponding to a 50 Ω transmission line.

added value. Moreover, losses in the wireless link, may limit the readability of the tag, especially if four-state S-SRR-based tags are considered, as mentioned before. Nevertheless, tag size and information capacity per GHz are the key aspects, and for that reason the four-state S-SRR based encoders are the preferred solution in this application (secure paper).

As a proof-of-concept, we have implemented spectral signature barcodes by etching eight S-SRRs on the commercial *Rogers RO4003C* substrate, with thickness h = 203 µm, dielectric constant ε_r = 3.55, and loss tangent $tan\delta$ = 0.0021, whereas the CPW transmission line has been implemented on the *Rogers RO4003C* substrate, with thickness h = 508 µm and same dielectric constant and loss tangent. In this proof-of-concept demonstrator, we have chosen a narrow substrate for S-SRR etching, similar to the typical flexible substrate required in a real application. The 3D views of the CPW and S-SRR (isolated) are depicted in Fig. 10. The tag is put on top of the CPW transmission line, with the S-SRRs etched on the substrate side opposite to the one in contact with the CPW of the reader. Additionally, we have considered a top dielectric slab (a commercial 0.81 mm thick *RO4003C* substrate with identical dielectric constant and loss tangent) in order to make pressure and thus minimize the effects of the air gap [33] as much as possible. The presence of this substrate has been taken into account in the design of the S-SRRs and tags. Note that in this case, the CPW transmission line is uniform (contrary to the previous four-state multi-resonator encoder). The reason is that since the S-SRRs are separated from the CPW transmission line by a very narrow substrate, the coupling level between line and resonant elements is high, and it is not necessary in this case to circularly shape the transverse dimensions of the line in the regions where the S-SRRs are present. It is worth mentioning that in our in-house measurement system (see Fig. 11), rather than a guiding channel for the tag, it has been positioned on top of the CPW and aligned to it by means of references (holes) drilled on the CPW and tag. Then, pressure to minimize the air gap has been done manually. The reader is the CPW connected to the two-port network analyzer.

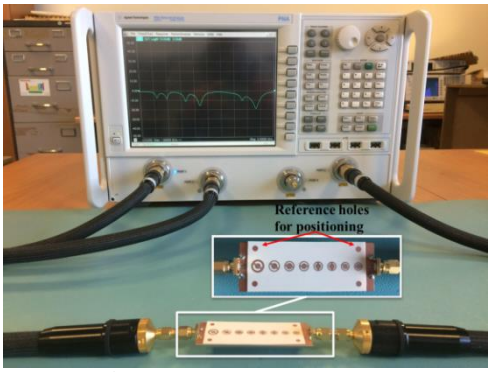

Fig. 11. Photograph of the experimental set-up.

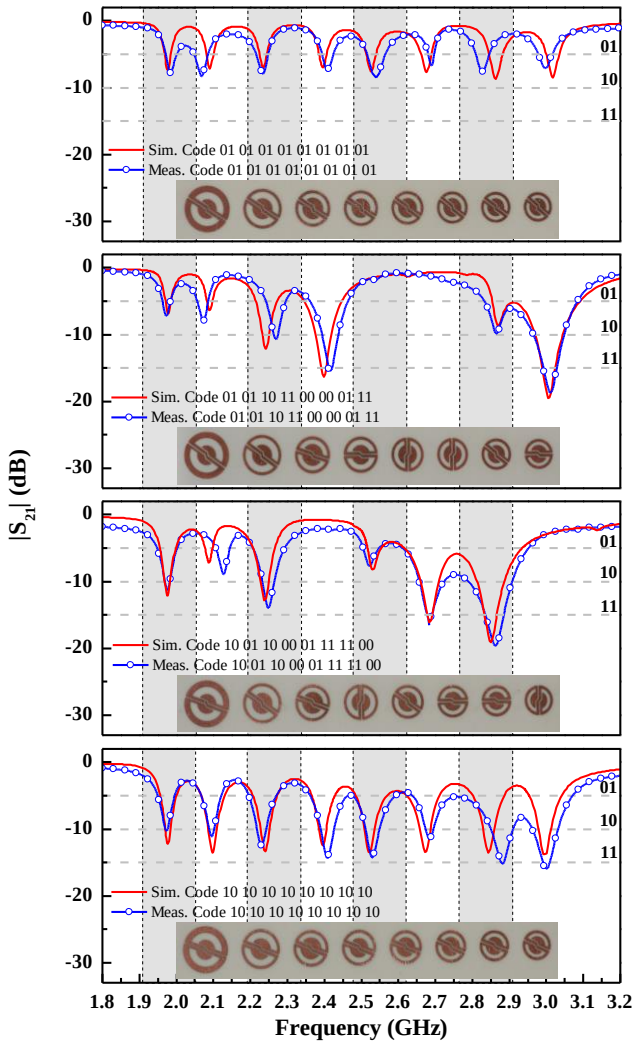

Fig. 12. Photograph and frequency responses of the four-state eight-resonator spectral signature barcodes with the indicated codes. In this case, the dimensions of the different S-SRRs have been obtained from the dimensions of the reference one by modifying the perimeter of the circular loop, as in the case of the tri-state 10-resonator barcodes of Section III.A. Note also that these photographs correspond actually to the barcodes after scaling, as mentioned in the text.

The dimensions of the reference resonator (with fundamental resonance frequency at 2.5 GHz) are indicated in the caption of Fig. 10, where the particle is depicted. The layouts and simulated frequency responses of four encoders are depicted in Fig. 12 (the codes are indicated in the figure). The intermediate states, designated by '01' and '10', are obtained by rotating the S-SRR 55º and 70º, respectively (providing equidistant notch depths) for rotation corresponding to the largest S-SRR can be

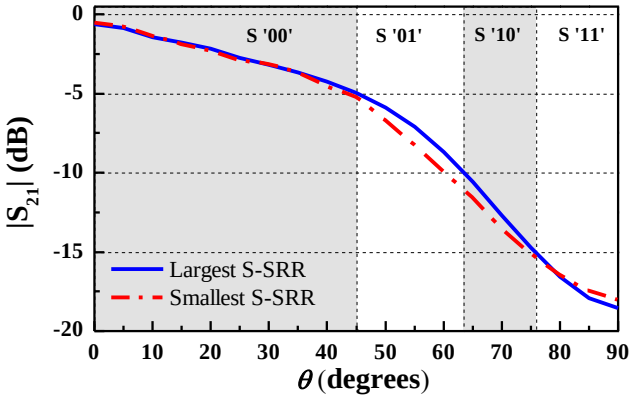

Fig. 13. Notch depth variation with the rotation angle for the extreme S-SRRs of the considered four-state eight-resonators tags.

appreciated in Fig. 13, where the notch depth as a function of the rotation angle is depicted (note that for the smallest S-SRR, the curve, also included, is roughly the same).

Due to the effects of the air gap (obviously not present in the simulation, but not completely suppressed in measurement), the measured responses have been found to shift 20% upwards (overall shift in the response). For this reason, we have scaled 20% up the dimensions of the S-SRRs and we have repeated the fabrication of the encoders. These new fabricated encoders exhibit the measured responses also depicted in Fig. 12, and their size is 75 mm × 9 mm.

The agreement between the measured responses of the different codes and those inferred from electromagnetic simulation is reasonably good, although the notch depths and resonance frequencies slightly change in some cases. The reason is the lack of an automatic and robust system in our in-house experimental set-up to accurately align and pressure the tags over the CPW and thus minimize the effects of misalignment and air gap. Nevertheless, these results demonstrate that the implementation and reading of four-state multi-resonator spectral signature barcodes, implemented in a different substrate than the host CPW line, is possible. Moreover, these results point out the possibility of implementing spectral signature-based chipless RFID systems with small tag size and significant number of bits. This has been achieved by avoiding the use of antennas and by considering multiple states per resonant element, thanks to the near-field reading (through inductive coupling) of the tags.

An important aspect affecting the bit error rate is the effect of lateral and vertical displacement (air gap) between the tag (S-SRRs) and the CPW transmission line. Thus, we have studied through electromagnetic simulation such effects on the variation of the notch depth and resonance frequencies. We have defined tolerance windows for both the notch depth and frequency. Specifically, since the distance between thresholds (notch depth) is 5 dB, the tolerance windows for the notch depth are considered to cover that range (i.e., 2.5 dB up and down). For the notch frequency, the windows are 142 MHz wide (71 MHz up and down) since this is the distance between adjacent resonance frequencies. In order to estimate the achievable tolerances in lateral and vertical displacement, we have considered the extreme cases of the largest (i.e., the lowest notch frequency) and smallest (the highest frequency) S-SRRs.

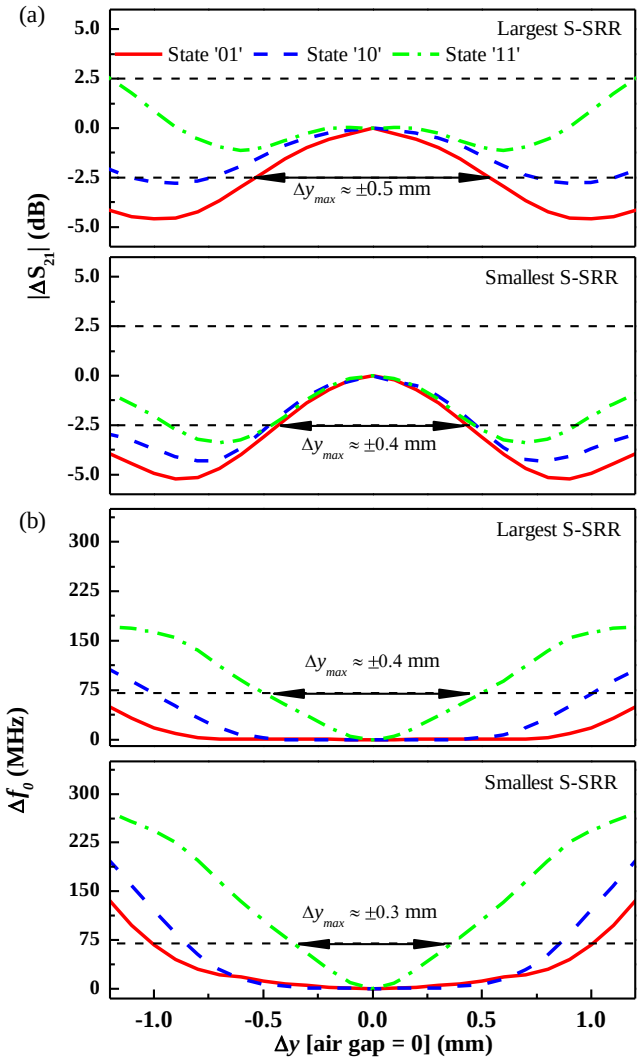

Fig. 14. Effects of lateral displacement on the notch depth (a) and frequency (b) for the extreme S-SRRs of Fig. 11 (before scaling).

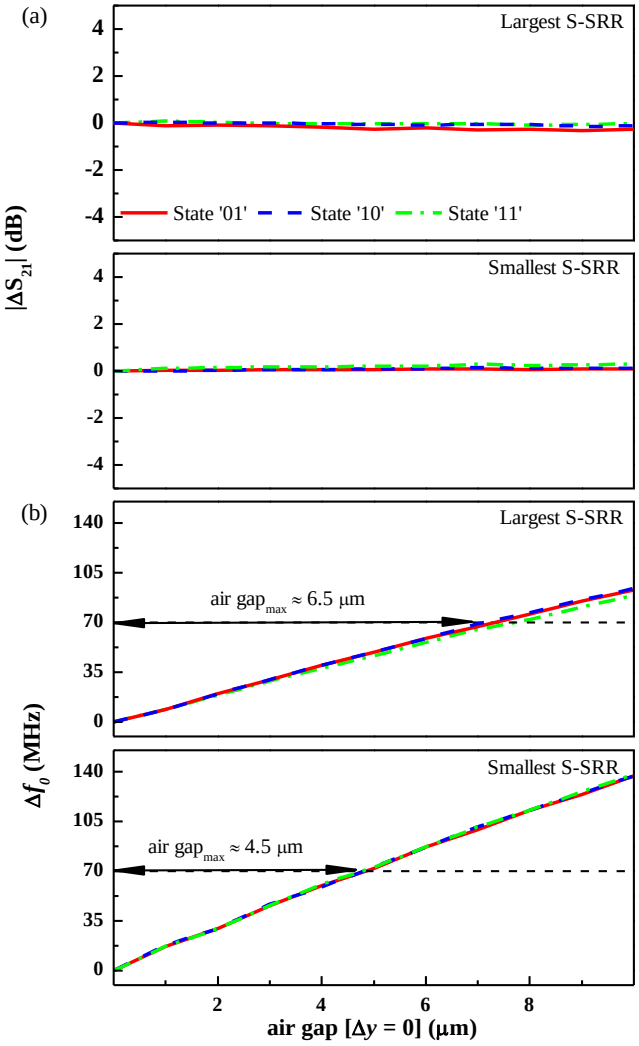

Fig. 15. Effects of vertical displacement (air gap) on the notch depth (a) and frequency (b) for the extreme S-SRRs of Fig. 11 (before scaling).

The variations of the notch depth and frequency with lateral displacement for states '01', '10' and '11' are depicted in Fig. 14 (note that state '00' is not relevant since the S-SRR is not excited regardless of the lateral or vertical displacement). With these results, we conclude that the maximum tolerance for lateral displacement is dictated by the frequency variation of state '11' of the smallest S-SRR, and it is 0.3 mm. For which concern the air gap (vertical displacement), its effects on notch variation in the considered range are negligible, but not on frequency variation (see Fig. 15). In this case, the tolerance is 4.5 μm, and this limit is dictated by the smallest S-SRR as well.

According to these results, the effects of vertical displacement are more critical. However, the idea in a real scenario is to make the measurement by contacting the CPW and tag under certain controllable pressure (i.e., by means of a mechanical system that displaces horizontally the tag until the position of the CPW, and then vertically to ensure contact and minimize the air gap, not completely unavoidable). Obviously this is not the case in our in-house set-up where, rather than a real guiding system, the tag is positioned and aligned on top of the CPW by means of references in both elements. With a reliable and robust guiding system (from a mechanical viewpoint) such value

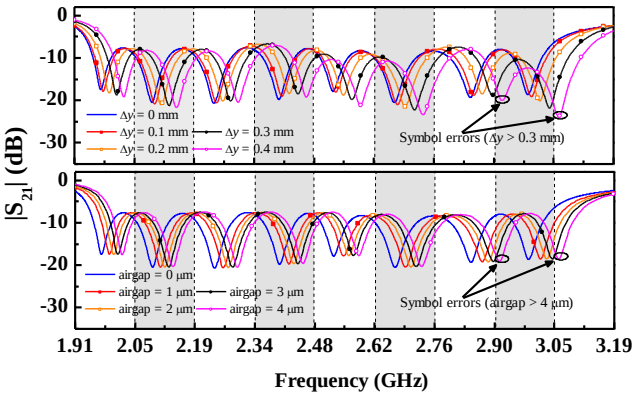

Fig. 16. Simulated responses of the four-state eight-resonators tag with all S-SRRs rotated 90º (all bits set to logic level '1') for different values of lateral displacement and air gap separation.

seems to be reasonable. For which concern lateral displacement (misalignment), in a hypothetical commercial system based on this approach, it seems reasonable to constrict the misalignment in less than 0.3 mm (less favorable case according to Fig. 14(b)). Alternatively, it is possible to further separate the resonance frequencies, but at the expense of a smaller number of bits per bandwidth. To further support the previous analysis, we report in Fig. 16 the responses of the tag with all resonators rotated 90º, for

TABLE IX
COMPARISON OF FREQUENCY-DOMAIN CHIPLESS TAGS

Ref.	Frequency range (GHz)	Number of bits	Tag area (cm^2)	DPF (bit/GHz)	DPS (bit/ cm^2)
[6]	3.1 - 7	35	57.2	8.97	0.61
[9]	0.7 - 0.9	5	50.1	25.0	0.10
[10]	5 - 6	5	6.48	11.1	0.77
[12]	2 - 4	20	17.5	10.0	1.14
[13]	2 - 5.5	9	3.00	2.57	3.00
[14]	3.1 - 10.6	19	9.00	2.53	2.11
[34]	2 - 5	9	7.20	3.00	1.25
[35]	3 - 10	28.5	8.00	4.07	3.56
[36]	3.2 - 9.6	64	10.9	10.0	5.88
[37]	3.1 - 10.6	24	5.76	3.20	4.17
[38]	1.9 - 3.1	20	17.5	16.7	1.14
[39]	2.5 - 7.5	22.9	8.00	4.58	2.86
Present work	**2 - 3**	**16**	**6.75**	**16.0**	**2.37**

different values of the lateral displacement and gap distance. Erroneous readings are visible and correspond to misalignments or air gaps beyond the tolerance values.

For the implementation of these tags in a polymer or paper, redesign S-SRRs taking into account the parameters of the substrate under consideration (thickness, dielectric constant and loss tangent) is necessary. The conductance of the conductive inks and the achievable thickness of the metallic films are additional important parameters that must be considered. For which concerns cost in a real scenario, industrial processes such as screen printing are preferred over inkjet (in spite that throughput has been recently improved), especially if many tags must be fabricated. This requires personalized masks for each code, which increases costs, but such costs may be affordable in applications where many replicas (typically hundreds or thousands) of the same code must be used (e.g., in corporate documents, identifying a person or a company, etc.).

IV. COMPARISON TO OTHER FREQUENCY-DOMAIN CHIPLESS TAGS

We have compared our near-field based chipless tags with other frequency domain chipless tags in terms of the used frequency range, number of bits, area, information density per frequency (DPF) and information density per surface (DPS). The results are shown in Table IX. The relevant parameters (or figures of merit) of these tags are those of the last two columns. In this regard, it is remarkable the work [9], where a huge DPF is obtained, but at the expense of a very large area (or low DPS). In [38], the DPF is comparable to the one reported in this work, but the DPS is roughly half the one achieved by us. It is also worth mentioning the work carried out in [36], where the authors achieve simultaneously good DPF and DPS. In our case, the DPF is substantially improved as compared to [36], but the DPS is not as good as in [36]. In summary, as compared to other frequency domain chipless tags, shown in Table IX, our proposal represents a very good balance between the achievable number of bits per bandwidth and per area unit.

V. CONCLUSIONS

In conclusion, multi-state (up to four states) multi-resonator spectral signature barcodes implemented by loading a host CPW transmission line with S-SRRs have been designed, fabricated, and characterized for the first time. The different states have been achieved by rotating the S-SRRs. This rotation (orientation) modulates the coupling level between the line and the resonators, thus varying the attenuation level in the transmission coefficient at the fundamental frequency of the considered resonator. After designing and implementing a three-state and a four-state multi-resonator encoder (using 10 and 9 S-SRRs, respectively) with the S-SRRs etched in the back substrate side of the CPW, we have implemented a four-state eight-resonator encoder where the S-SRRs have been etched in a different substrate. This has opened a new paradigm in spectral signature based chipless RFID, where the tag is simply the set of S-SRRs etched (or printed) in the considered substrate (it can be a flexible substrate or even paper, in a real scenario), the CPW transmission line is an essential part (active part) of the reader, and the communication between the tag and the reader is by inductive coupling. This requires good alignment and contact between the tag and the reader, but this is possible in certain applications, especially those related to security and authentication, as has been discussed in the paper. By this means, antennas are avoided, with direct impact on tag size. Additionally, it has been experimentally demonstrated that by means of this approach, the four states can be discriminated. The proof-of-concept has been implemented by considering a narrow commercial microwave substrate with moderate dielectric constant (3.55) for the S-SRRs, i.e., conditions similar to those of flexible substrates. Work is in progress towards the implementation of multi-state multi-resonator encoders in such substrates by means of printed techniques.

REFERENCES

[1] K. Finkenzeller, *RFID Handbook: Radio-Frequency Identification Fundamentals and Applications*, 2nd ed., John Wiley, New York, 2004.

[2] V.D. Hunt, A. Puglia, and M. Puglia, *RFID: A Guide to Radiofrequency Identification*, John Wiley, New York, 2007.

[3] S. Preradovic and N. C. Karmakar, "Chipless RFID: bar code of the future," *IEEE Microwave Magazine*, vol. 11, no. 7, pp. 87-97, 2010.

[4] E. Perret, *Radio Frequency Identification and Sensors: From RFID to Chipless RFID*, John Wiley, New York, 2014.

[5] R. Rezaiesarlak and M. Manteghi, *Chipless RFID: Design Procedure and Detection Techniques*, Springer, 2015.

[6] S. Preradovic, I. Balbin, N. C. Karmakar, and G. F. Swiegers, "Multiresonator-based chipless RFID system for low-cost item tracking," *IEEE Trans. Microw. Theory Techn.*, vol. 57, no. 5, pp. 1411-1419, 2009.

[7] S. Preradovic and N. C. Karmakar, "Design of chipless RFID tag for operation on flexible laminates," *IEEE Anten. Wireless Propag. Lett.*, vol. 9, pp. 207-210, 2010.

[8] S. Preradovic and N. C. Karmakar, *Multiresonator-based Chipless RFID: Barcode of the Future*, Springer, 2012.

[9] J. McVay, A. Hoorfar, and N. Engheta, "Space-filling curve RFID tags," in *IEEE Radio Wireless Symp.*, pp. 199–202, 2006.

[10] I. Jalaly and D. Robertson, "Capacitively-tuned split microstrip resonators for RFID barcodes," in *European Microwave Conference*, October 2005, vol. 2, pp. 4–7, 2005.

[11] H.-S. Jang, W.-G. Lim, K.-S. Oh, S.-M. Moon, and J.-W. Yu, "Design of low-cost chipless system using printable chipless tag with electromagnetic code," *IEEE Microw. Wireless Compon. Lett.*, vol. 20, no. 11, pp. 640-642, 2010.

[12] A. Vena, E. Perret, and S. Tedjini, "A fully printable chipless RFID tag with detuning correction technique," *IEEE Microw. Wireless Compon. Lett.*, vol. 22, no. 4, pp. 209-211, 2012.

[13] A. Vena, E. Perret, and S. Tedjini, "Design of compact and auto-compensated single-layer chipless RFID tag," *IEEE Trans. Microw. Theory Techn*., vol. 60, no. 9, pp. 2913-2924, Sept. 2012.
[14] A. Vena, E. Perret, and S. Tedjini, "High-capacity chipless RFID tag insensitive to the polarization," *IEEE Trans. Ant. Propag.*, vol. 60, no. 10, pp. 4509-4515, Oct. 2012.
[15] C. S. Hartmann, "A global SAW ID tag with large data capacity," in *IEEE Ultrasonics Symposium*, October 2002, vol. 1, pp. 65–69.
[16] A. Chamarti and K. Varahramyan, "Transmission delay line based ID generation circuit for RFID applications," *IEEE Microw. Wireless Compon. Lett.*, vol. 16, no. 11, pp. 588-590, 2006.
[17] M. Schüßler, C. Damm, and R. Jakoby, "Periodically LC loaded lines for RFID backscatter applications," in *Metamaterials*, October 2007, pp. 103-106.
[18] M. Schüßler, C. Damm, M. Maasch, and R. Jakoby, "Performance evaluation of left-handed delay lines for RFID backscatter applications," in *IEEE MTT-S International Microwave Symposium*, 2008, pp. 177-180.
[19] F.J. Herraiz-Martínez, F. Paredes, G. Zamora, F. Martín, and J. Bonache, "Printed magnetoinductive-wave (MIW) delay lines for chipless RFID applications," *IEEE Trans. Ant. Propag.*, vol. 60, no. 11, pp. 5075-5082, Nov. 2012.
[20] C. Herrojo, J. Naqui, F. Paredes, F. Martín, "Spectral signature barcodes implemented by multi-state multi-resonator circuits for chipless RFID tags," *IEEE MTT-S International Microwave Symposium* (IMS), May 2016, pp. 1-4.
[21] H. Chen, L. Ran, J. Huangfu, X. Zhang, K. Chen, T. M. Grzegorczyk, and J. A. Kong, "Left-handed materials composed of only S-shaped resonators," *Phys. Rev. E*, vol. 70, no. 5, pp. 1-4, Nov. 2004.
[22] H. Chen, L. Ran, J. Huangfu, X. Zhang, K. Chen, T. M. Grzegorczyk, and J. A. Kong, "Negative refraction of a combined double S-shaped metamaterial," *Appl. Phys. Lett.*, vol. 86, no. 15, p. 151909, 2005.
[23] H. Chen, L.-X. Ran, H.-F. Jiang Tao, X.-M. Zhang, K.-S. Cheng, T. M Grzegorczyk, and J. A. Kong, "Magnetic properties of S-shaped split ring resonators," *Prog. Electromagn. Res.*, vol. 51, pp. 231–247, 2005.
[24] J. Naqui, J. Coromina, A. Karami-Horestani, C. Fumeaux, and F. Martín, "Angular displacement and velocity sensors based on coplanar waveguides (CPWs) loaded with S-shaped split ring resonator (S-SRR)," *Sensors*, vol. 15, no. 5, pp. 9628-9650, 2015.
[25] F. Martin, *Artificial Transmission Lines for RF and Microwave Applications*, John Wiley, Hoboken, NJ, USA, 2015.
[26] J. Naqui, *Symmetry properties in transmission lines loaded with electrically small resonators: circuit modeling and applications*, Springer, 2016.
[27] J. Naqui, M. Durán-Sindreu, and F. Martín, "Novel Sensors Based on the Symmetry Properties of Split Ring Resonators (SRRs)," *Sensors*, vol 11, pp. 7545-7553, 2011.
[28] J. Naqui and F. Martín, "Transmission lines loaded with bisymmetric resonators and their application to angular displacement and velocity sensors," *IEEE Trans. Microw. Theory Techn.*, vol. 61, no. 12, pp. 4700-4713, Dec. 2013.
[29] A.K. Horestani, D. Abbott, and C. Fumeaux, "Rotation sensor based on horn-shaped split ring resonator," *IEEE Sens. J.*, vol. 13, no. 8, pp. 3014–3015, 2013.
[30] J. Naqui and F. Martín, "Angular displacement and velocity sensors based on electric-LC (ELC) loaded microstrip lines," *IEEE Sensors J.*, vol. 14, no. 4, pp. 939-940, Apr. 2014.
[31] D. Schurig, J. J. Mock, and D. R. Smith, "Electric-field-coupled resonators for negative permittivity metamaterials," *Appl. Phys. Lett*., vol. 88, no. 4, 2006.
[32] F. Aznar, M. Gil, J. Bonache, J.D. Baena, L. Jelinek, R. Marqués, and F. Martín, "Characterization of miniaturized metamaterial resonators coupled to planar transmission lines," *J. Appl. Phys*., vol. 104, paper 114501-1-8, Dec. 2008.
[33] C. Yang, C. Lee, K. Chen, and K. Chen, "Noncontact measurement of complex permittivity and thickness by using planar resonators," *IEEE Trans. Microw. Theory Techn*., vol. 64, no. 1, pp. 247-257, Jan. 2016.
[34] O. Rance, R. Siragusa, P. Lemaître-Auger, and E. Perret, "Toward RCS magnitude level coding for chipless RFID," *IEEE Trans. Microw. Theory Techn.*, vol. 64, no. 7, pp. 2315-2325, Jul. 2016.
[35] M. M. Khan, F. A. Tahir, M. F. Farooqui, A. Shamim, and H. M. Cheema., "3.56-bits/cm^2 compact inkjet printed and application specific chipless RFID tag," *IEEE Ant. Wireless Propag. Lett.*, vol. 15, pp. 1109-1112, 2016.
[36] M. A. Islam and N. C. Karmakar, "A novel compact printable dual-polarized chipless RFID system," *IEEE Trans. Microw. Theory Techn.*, vol. 60, no. 7, pp. 2142-2151, Jul. 2012.
[37] R. Rezaiesarlak and M. Manteghi, "Complex-natural-resonance-based design of chipless RFID tag for high-density data," *IEEE Trans. Ant. Propag*., vol. 62, no. 2, pp. 898-904, Feb. 2014.
[38] M. Svanda, J. Machac, M. Polivka, and J. Havlicek., "A comparison of two ways to reducing the mutual coupling of chipless RFID tag scatterers," in *21st International Conference on Microwave, Radar and Wireless Communications (MIKON)*, May 2016, pp. 1-4.
[39] A. Vena, E. Perret, and S. Tedjini, "Chipless RFID tag using hybrid coding technique," *IEEE Trans. Microw. Theory Techn.*, vol. 59, no. 12, pp. 3356-3364, Dec. 2011.

Cristian Herrojo was born in Badalona (Barcelona), Spain, in 1983. He received the Telecommunications Technical Engineering degree (specialty in Electronic Systems) and the Telecommunications Engineering degree in 2010 and 2012, respectively. Currently, he is working toward his PhD which is mainly focused on the design of RF/microwave resonant structures applied to RFID tags (Radio Frequency Identification) without chip and he has a research grant from FPI Program of the Education and Science Spanish Ministry.

Ferran Paredes was born in Badalona (Barcelona), Spain in 1983. He received the Telecommunications Engineering Diploma (specializing in Electronics) and the Telecommunications Engineering degree from the Universitat Autònoma de Barcelona in 2004 and 2006, respectively and the PhD degree in Electronics Engineering from the same university in 2012. He was Assistant Professor from 2006 to 2008 at the Universitat Autònoma de Barcelona, where he is currently working as a Research Assistant. His research interests include metamaterial concepts, passive microwaves devices, antennas and RFID.

Javier Mata-Contreras was born in 1976 in Málaga (Spain). He received the Ingeniería de Telecomunicación Degree from the Universidad de Málaga (UMA) in 2000 and the PhD degree from the same university in 2010, with the Thesis "Distributed Amplifiers and Mixers with Transmission Lines based on Metamaterials". In 2000, he joined the UMA Department of Ingeniería de Comunicaciones UMA as Assistant Professor. He is currently working at CIMITEC and the Universitat Autònoma de Barcelona as Visitant Professor. His research interests include active and passive microwave devices and active distributed circuits based on metamaterials, among others.

Simone Zuffanelli was born in Prato (Italy) in 1983. He received the Electronics Engineering Diploma in 2008 at the Università Degli Studi di Firenze. He obtained "Micro and Nanoelectronics Engineering" master's degree in 2011 at the Universitat Autònoma de Barcelona. He is currently working as a researcher in the field of metamaterial inspired antennas and RFID tags. His previous experiences include electronic design in the context of European projects "Persona" and "NOMS".

Ferran Martín (M'04-SM'08-F'12) was born in Barakaldo (Vizcaya), Spain in 1965. He received the B.S. Degree in Physics from the Universitat Autònoma de Barcelona (UAB) in 1988 and the PhD degree in 1992. From 1994 up to 2006 he was Associate Professor in Electronics at the Departament d'Enginyeria Electrònica (Universitat Autònoma de Barcelona), and since 2007 he is Full Professor of Electronics. In recent years, he has been involved in different research activities including modelling and simulation of electron devices for high frequency applications, millimeter wave and THz generation systems, and the application of electromagnetic bandgaps to microwave and millimeter

wave circuits. He is now very active in the field of metamaterials and their application to the miniaturization and optimization of microwave circuits and antennas. He is the head of the Microwave Engineering, Metamaterials and Antennas Group (GEMMA Group) at UAB, and director of CIMITEC, a research Center on Metamaterials supported by TECNIO (Generalitat de Catalunya). He has organized several international events related to metamaterials, including Workshops at the IEEE International Microwave Symposium (years 2005 and 2007) and European Microwave Conference (2009), and the Fifth International Congress on Advanced Electromagnetic Materials in Microwaves and Optics (Metamaterials 2011), where he has acted as chair of the Local Organizing Committee. He has acted as Guest Editor for three Special Issues on Metamaterials in three International Journals. He has authored and co-authored over 500 technical conference, letter, journal papers and book chapters, he is co-author of the book on Metamaterials entitled *Metamaterials with Negative Parameters: Theory, Design and Microwave Applications* (John Wiley & Sons Inc. 2008), author of the book *Artificial Transmission Lines for RF and Microwave Applications* (John Wiley & Sons Inc. 2015), and he has generated 16 PhDs. Ferran Martín has filed several patents on metamaterials and has headed several Development Contracts.

Prof. Martín is a member of the IEEE Microwave Theory and Techniques Society (IEEE MTT-S). He is reviewer of the IEEE Transactions on Microwave Theory and Techniques and IEEE Microwave and Wireless Components Letters, among many other journals, and he serves as member of the Editorial Board of IET Microwaves, Antennas and Propagation and International Journal of RF and Microwave Computer-Aided Engineering. He is also a member of the Technical Committees of the European Microwave Conference (EuMC) and International Congress on Advanced Electromagnetic Materials in Microwaves and Optics (Metamaterials). Among his distinctions, Ferran Martín has received the 2006 Duran Farell Prize for Technological Research, he holds the *Parc de Recerca UAB – Santander* Technology Transfer Chair, and he has been the recipient of two ICREA ACADEMIA Awards (calls 2008 and 2013). He is Fellow of the IEEE since 2012 and Fellow of the IET since 2016.